Coupled phonons, magnetic excitations, and ferroelectricity in $AlFeO_3$: Raman and first-principles studies

Pradeep Kumar,[1] Achintya Bera,[1] D. V. S. Muthu,[1] Sharmila N. Shirodkar,[2] Rana Saha,[3] Ajmala Shireen,[3] A. Sundaresan,[3] U. V. Waghmare,[2] A. K. Sood,[1,*] and C. N. R. Rao[3]

[1]*Department of Physics, Indian Institute of Science, Bangalore 560012, India*

[2]*Theoretical Sciences Unit, Jawaharlal Nehru Centre for Advanced Scientific Research, Jakkur P.O., Bangalore 560064, India*

[3]*Chemistry and Physics of Materials Unit, New Chemistry Unit and International Centre for Materials Science, Jawaharlal Nehru Centre for Advanced Scientific Research, Jakkur P.O., Bangalore 560064, India*

(Received 18 December 2011; revised manuscript received 21 February 2012; published 27 April 2012)

We determine the nature of coupled phonons and magnetic excitations in $AlFeO_3$ using inelastic light scattering from 5 to 315 K covering a spectral range from 100 to 2200 cm^{-1} and complementary first-principles density functional theory–based calculations. A strong spin–phonon coupling and magnetic ordering–induced phonon renormalization are evident in (1) anomalous temperature dependence of many modes with frequencies below 850 cm^{-1}, particularly near the magnetic transition temperature $T_c \approx 250$ K, and (2) distinct changes in band positions of high-frequency Raman bands between 1100 and 1800 cm^{-1}; in particular, a broad mode near 1250 cm^{-1} appears only below T_c, attributed to the two-magnon Raman scattering. We also observe weak anomalies in the mode frequencies ∼100 K due to a magnetically driven ferroelectric phase transition. Understanding of these experimental observations has been possible on the basis of first-principles calculations of the phonons' spectrum and their coupling with spins.

DOI: 10.1103/PhysRevB.85.134449 PACS number(s): 63.20.kk

I. INTRODUCTION

Materials that exhibit co-occurrence of both magnetic and ferroelectric order parameters have generated enormous interest in recent years because of fundamental issues related to the coupling among spin, orbital, charge, and lattice degrees of freedom, as well as because of their potential applications.[1–5] For applications, it is desirable to have materials with magnetoelectric properties around room temperature, which is not realized in many magnetoelectric materials in which magnetic ordering is the primary driving force. In this context, $AlFeO_3$ exhibiting ferrimagnetism and possible magnetoelectric coupling is promising, with a paramagnetic to ferrimagnetic (FM) transition temperature $T_c \approx 250$ K.[6,7] Another attractive feature is the environment friendly nature of $AlFeO_3$ as compared to other lead-based multiferroics.

In $AlFeO_3$, cations occupy four distinct crystallographic sites: cations Fe_1, Fe_2, and Al_2 are octahedrally coordinated by oxygen, whereas Al_1 is tetrahedrally coordinated. Structural analysis of $AlFeO_3$[7] shows significant distortion of the FeO_6 octahedra, while the oxygen tetrahedron around Al_1 is quite regular. The cause for the local deformation of lattice has been attributed to the difference between octahedral radii of Fe^{3+} and Al^{3+} ions and the disorder in the occupation of octahedral cation sites. Vibrational properties, which bear signatures of structure and magnetic order, are central to magnetoelectric behavior of many multiferroics. In particular, Raman spectroscopy has proved a powerful probe to investigate magnetic ordering–induced phonon renormalization, where the observed phonon anomalies below the magnetic transition temperature have been associated with the strong spin–phonon coupling.[8–11]

There is no report so far of a Raman study of $AlFeO_3$. However, on a related system, $GaFeO_3$, first-order Raman modes are reported,[12,13] and the observed modes show anomalous temperature dependence near T_c (∼210 K) attributed to the spin–phonon interactions. In this paper, we report a detailed temperature-dependent Raman study of $AlFeO_3$ ($T_c \approx$ 250 K) with a goal to understand the phonon renormalization due to spin–phonon coupling in a magnetically ordered state below T_c. We have also looked for phonon signatures of a ferroelectric transition ∼100 K arising from magnetic interactions.[14] Our study covers first-order, as well as high-frequency second-order and two-magnon, Raman scattering. Taking inputs from first-principles density functional theory (DFT)–based calculations of phonons in different magnetically ordered $AlFeO_3$, our temperature-dependent Raman study reveals strong phonon renormalization below T_c, and its origin in the strong spin–phonon coupling and a coupling between two-phonon modes and magnetic excitation.

II. METHODS

A. Experimental details

Polycrystalline samples of $AlFeO_3$ were prepared and characterized as described in Ref. 15. Unpolarized micro-Raman measurements were performed on a polycrystalline pellet of $AlFeO_3$ in backscattering geometry using the 514.5-nm line of an Ar-ion laser (Coherent Innova 300) and Raman spectrometer (Dilor XY) coupled to a liquid nitrogen–cooled charge-coupled device detector. Temperature variation was done from 5 to 315 K, with a temperature accuracy of ± 0.1 K using a continuous-flow He cryostat (Oxford Instruments).

B. Computational details

Our first-principles calculations are based on DFT with the spin density–dependent exchange correlation energy functional of a generalized gradient approximation (PerdewWang 91) form,[16] as implemented in the Vienna *ab initio* simulation package.[17,18] The projector-augmented wave method[19] was used to capture interaction between ionic cores and valence

electrons. An energy cutoff of 400 eV was used for the plane wave basis, and integrations over the Brillouin zone of the orthorhombic crystal were sampled with a regular 4 × 2 × 2 mesh of k-points. Dynamical matrix and phonons at the Γ-point (q = 0,0,0) were obtained with a frozen-phonon method with atomic displacements of ±0.04 Å. Numerical errors in our calculations break the symmetry of the dynamical matrix weakly and introduce an error of about ±12 cm^{-1} in the phonon frequencies.

III. RESULTS AND DISCUSSIONS

A. Raman scattering from phonons

$AlFeO_3$ has a layered structured belonging to the orthorhombic $Pna2_1$ space group containing eight formula units, i.e., 40 atoms in a unit cell, resulting in 120 normal modes, namely, $\Gamma_{Fe} = 6A_1 + 6A_2 + 6B_1 + 6B_2$, $\Gamma_{Al} = 6A_1 + 6A_2 + 6B_1 + 6B_2$, and $\Gamma_o = 18A_1 + 18A_2 + 18B_1 + 18B_2$.[12] Because the inversion symmetry is lacking, Raman modes are also infrared active. There are 117 Raman modes, while $A_1 + B_1 + B_2$ are acoustic modes. Figure 1 shows the Raman spectrum at 5 K, revealing 18 modes labeled as S1 to S18 in the spectral range of 100–2200 cm^{-1}. Spectra are fitted with a sum of Lorentzian functions; the individual modes are shown by thin lines, and the resultant fit is shown by a thick line. Our first-principles density functional calculations (discussed later) suggest that the first-order Raman phonons occur below ∼810 cm^{-1}. Table I lists the experimental (at 5 K); the calculated frequencies for the disordered antiferromagnetic (AFM) state close to the experimental values are also listed. Because the intensity of mode S15 is zero above T_c, it is attributed to two-magnon Raman scattering (to be discussed later). Modes S16–S18 are assigned to second-order Raman scattering coupled with magnetic degrees of freedom.

B. Temperature dependence of the first-order phonons

Figure 2 shows the mode frequencies of some prominent first-order phonon modes (S4, S7–S10, S13, and S14) as a function of temperature. Three observations can be made. First, the frequencies of modes S4, S7–S10, and S13 show a sharp change at T_c. The temperature derivative of the frequencies of modes S4 and S10 ($\partial\omega/\partial T$) changes signs at T_c. In addition, the frequency of mode S13 shows a jump by ∼4 cm^{-1} near

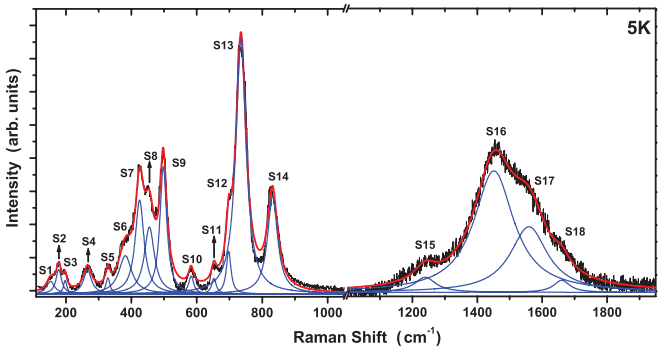

FIG. 1. (Color online) Unpolarized Raman spectra of $AlFeO_3$ at 5 K. Solid thin lines are the fit of individual modes, and solid thick line shows the total fit to the experimental data.

TABLE I. Experimental observed frequencies at 5 K and calculated frequencies in $AlFeO_3$ for the disordered AFM (Fe_2-Al_2 antisite disorder) state.

Mode assignment	Experimental ω (cm^{-1})	Calculated ω (cm^{-1})
S1	156	154
S2	178	179
S3	198	197
S4	268	270
S5	328	331
S6	380	379
S7	425	425
S8	453	453
S9	498	499
S10	587	581
S11	650	654
S12	698	691
S13	738	733
S14	826	807
S15 (two magnon)	1240	
S16 (overtone)	1450	
S17 (second order)	1560	
S18 (overtone)	1660	

T_c. Second, the slope of ω with respect to temperature for modes S4, S8–S10, and S14 shows changes near 100 K. We attribute these changes to a ferroelectric transition in this system ∼100 K, because the pyroelectric experiments showed[14] that a polar phase exits below ∼100 K and the reversal of polarization data with the changing direction of

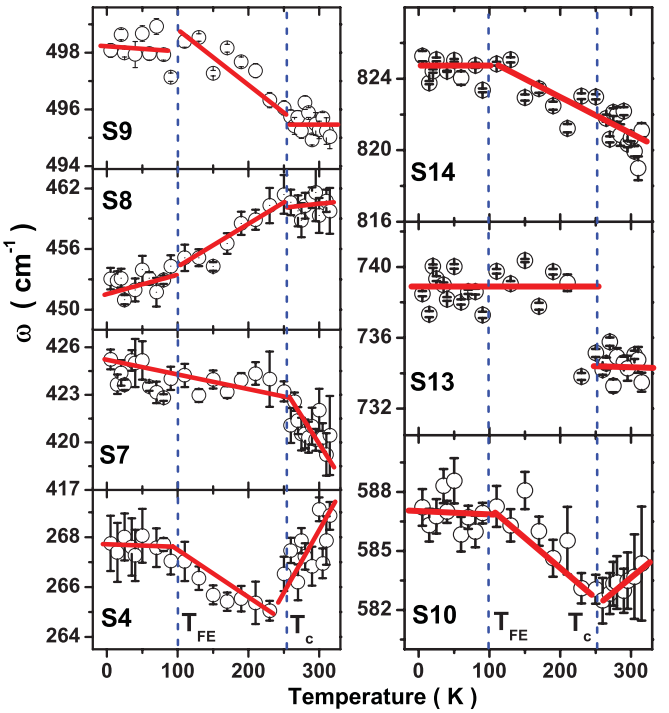

FIG. 2. (Color online) Temperature dependence of the first-order phonon modes S4, S7–S10, S13, and S14. Solid lines are the linear fits in three temperature regions, as described in the text.

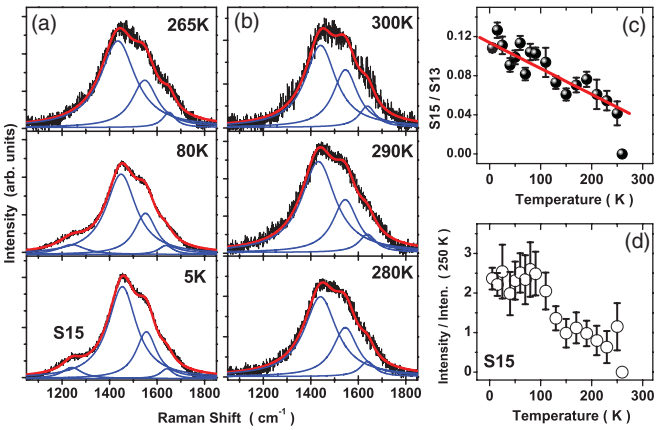

FIG. 3. (Color online) (a and b) Temperature evolution of mode S15 at a few typical temperatures. (c) Intensity ratio of the S15 mode with respect to the prominent first-order S13 mode. The solid line is the linear fit. (d) Temperature dependence of the intensity of the S15 mode with respect to its intensity at 250 K.

the electric field during pyroelectric current measurement demonstrates that the material is indeed a ferroelectric. The solid lines in the Fig. 2 panels are linear fits in three regions, i.e., 315–250 K, 250–100 K, and 100–5 K. Third, the temperature dependence of mode S8 is anomalous below T_c; i.e., frequency decreases on lowering the temperature.

The anomalies in the temperature dependence of phonon modes S4 and S7–S10 near T_c are similar to those in RMnO$_3$ (R = Pr, Nd, Sm, Tb, Dy, and La), GaFeO$_3$, and BiFeO$_3$.[8,10–13,20–23] The sharp change in the frequency of mode S13 at T_c can arise from a subtle local structural change. Following manganites[8,10–13,20–23] and our theoretical calculations, the sharp changes in mode frequencies of S4 and S7–S10 are attributed to strong spin–phonon coupling in the magnetic phase below T_c.

C. High-frequency modes: second-order phonon and magnon scattering

Two-phonon Raman bands are related to two-phonon density of states that have contributions from all branches in the first Brillouin zone. For simplicity, we fitted the high-energy Raman band (1100–1800 cm^{-1}) with a sum of four Lorentzian modes (S15–S18), where peak positions represent maxima in the two-phonon density of states. Because the second-order Raman scattering involves the phonons over the entire Brillouin zone, the frequencies of the observed second-order phonons are not necessarily double those of the first-order phonons at the Γ-point (q = 0,0,0). Accordingly, mode S17 can be assigned as a combination of S13 and S14, mode S16 as an overtone of mode S13, and mode S18 as an overtone of mode S14.

Figures 3(a) and 3(b) shows the high-frequency modes at a few typical temperatures. It can be seen that mode S15 is absent in the spectrum recorded at and above 265 K. Figure 3(d) shows the integrated intensity of the S15 mode with respect to its intensity at 250 K. Taking mode S13 as an internal marker, Fig. 3(c) shows the intensity of mode S15 with respect to that of mode S13. The intensity of mode S15

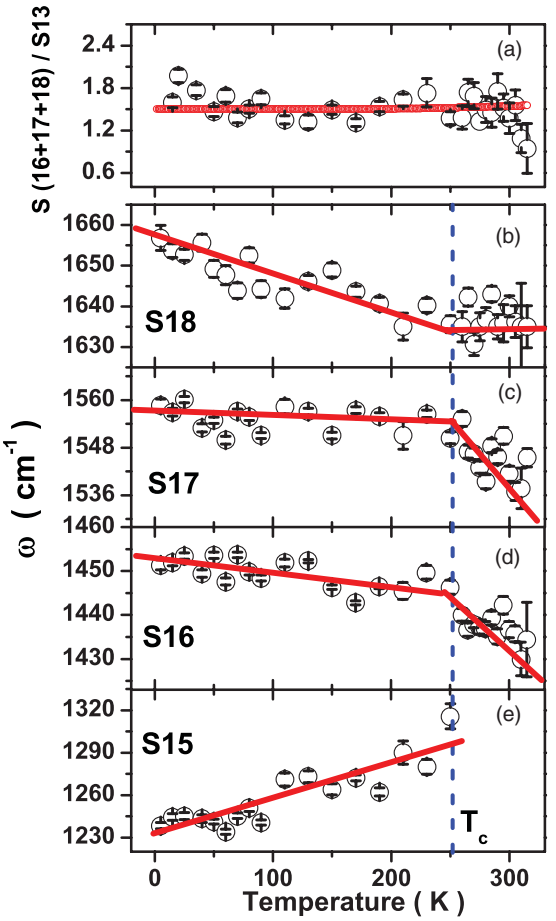

FIG. 4. (Color online) (a) Intensity ratio of the high-frequency band with respect to the prominent first-order mode. The solid line is the fitted curve as described in the text. (b–e) Temperature dependence of modes S15–S18. Solid lines are linear fits below and above T_c.

is zero above T_c, and its intensity builds up as we lower the temperature. The vanishing of the S15 mode above 250 K suggests that it can be associated with two-magnon Raman scattering. From the energy of the two-magnon band, an estimate of the nearest-neighbor exchange coupling parameter J_o can be made. If spins deviations are created on the adjacent sites, the two-magnon energy is given by $J_o(2Sz - 1)$, where S is the spin on the magnetic site (Fe^{3+} here, with S = 5/2) and z (z = 6) is the number of the nearest neighbor to that site.[24] Using ω = 1240 cm^{-1} (at 5 K), the estimated value of the exchange parameter J_o is ∼5.3 meV. This value is close to our first-principles calculations of $J_o \approx 6$ meV (discussed later). As temperature is lowered below T_c, the S15 mode frequency decreases significantly (∼5%) [Fig. 4(e)]. The frequencies of modes S16–S18 show a change in $\partial\omega/\partial T$ near the transition temperature [Fig. 4(b)–4(d)], attributed to the possible coupling between two-phonon and magnetic excitations similar to that in other magnetic systems.[8,11,20–30]

To ascertain the second-order nature of high-frequency bands S16–S18, we plot in Fig. 4(a) the sum of their intensities with respect to the intensity of the dominant first-order S13 mode. The second-order Raman intensity for a combination mode of frequency $(\omega_1 + \omega_2)$ is $[n(\omega_1) + 1][n(\omega_2) + 1]$, where $n(\omega)$ is the Bose-Einstein mean occupation number. The

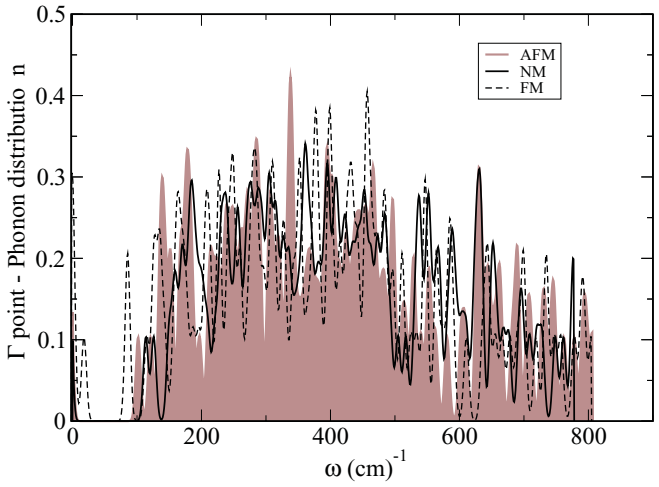

FIG. 5. (Color online) Distribution of phonons at Γ-point for AFM, FM, and NM orderings with a Gaussian broadening of ∼4 cm^{-1}.

ratio of the second-order band with respect to the first-order mode of frequency ω_1 is $c[n(\omega_2)+1]$, where c is the ratio depending on the matrix elements in second- and first-order Raman scattering. The solid line in Fig. 4(a) is $1.5^*[n(\omega = 740\,cm^{-1})+1]$, showing that the broad band (decomposed into modes S16–S18) is due to second-order Raman scattering. We now develop a theoretical understanding of our results.

D. First-principles calculations

It is known[7] that $AlFeO_3$ has a site occupancy disorder between the Fe and the Al sites, with the most common occurrence of antisite disorder between the Fe_2 and the Al_2 sites.[7] This disorder is taken into account by exchanging the site position of an Fe atom at the Fe_2 site with that of an Al atom at the Al_2 site. We also considered antisite disorder between the Fe_1 and the Al_2 sites. From the energetics, we found that the AFM state is the most stable for a system with either type of antisite disorder between Fe and Al. The AFM state with Fe_1-Al_2 antisite disorder is higher in energy, compared to the AFM state with Fe_2-Al_2 antisite disorder, by 5.7 meV/atom, confirming the higher occurrence of Fe_2-Al_2 antisite disorder. To facilitate a meaningful comparison with experimental Raman spectra, we simulate the structure with experimental lattice constants, internally relaxing the atomic positions using conjugate gradients algorithm.

To understand the interplay among disorder, magnetic ordering, and phonons, we determine phonons at Γ-point for a chemically disordered structure with nonmagnetic (NM), FM, and AFM ordering (Fig. 5). The spin–phonon coupling is analyzed by examining how normal modes depend on the magnetic ordering, which is done in turn by examining the correlation matrix between phonon eigenmodes of $AlFeO_3$ in two different magnetically ordered states. In the absence of spin–phonon coupling, the phonons would be unaffected by changes in the magnetic order; hence, only the diagonal terms would be nonzero in the correlation matrix. Nonzero off-diagonal elements of the correlation matrix clearly uncover the correspondence between eigenmodes in different magnetic orders. For example, these elements determine which phonon modes of the AFM state relate to phonons of the FM state, giving a quantitative idea of mixing between modes due to spin–phonon coupling.

The spin-Hamiltonian has the form

$$H = \frac{1}{2}\sum_{ij} J_{ij}\vec{S}_i.\vec{S}_j, \tag{1}$$

where J_{ij} is the exchange interaction between the ith- and the jth-izing spins S_i and S_j. Only considering the nearest neighbor and isotropic interaction, we reduce J_{ij} to J. The change in J due to spin–phonon coupling is given by second-order Taylor series expansion of J with respect to amplitude of atomic displacements ($u_{\nu\Gamma}$) of the νth Γ-phonon mode of the magnetic state,[20]

$$J(u_{\nu\Gamma}) = J_o + \vec{u}_{\nu\Gamma}(\nabla_u J) + \tfrac{1}{2}\vec{u}_{\nu\Gamma}\left(\nabla_u^2 J\right)\vec{u}_{\nu\Gamma}. \tag{2}$$

Summing over all modes gives

$$H = \frac{1}{2}\sum_{\nu}\sum_{ij}\left[J_o + \vec{u}_{\nu\Gamma}(\nabla_u J) + \frac{1}{2}\vec{u}_{\nu\Gamma}\left(\nabla_u^2 J\right)\vec{u}_{\nu\Gamma}\right].\vec{S}_i\vec{S}_j\,. \tag{3}$$

Here, J_o is the bare spin–spin coupling parameter, $\nabla_u J$ corresponds to the force exerted on the system due to change in magnetic ordering from its ground state magnetic configuration, and $\nabla_u^2 J$ is proportional to the change in phonon frequency Δ of the νth Γ-phonon mode due to change in magnetic ordering. From the spin–Hamiltonian (Eq. (1)), energies of a single pair of spins in AFM and FM states are given by $E_{\rm AFM} = -J_o\,|S|^2$ and $E_{\rm FM} = J_o\,|S|^2$, respectively. The difference in the energies of AFM and FM states is directly proportional to J_o. The unit cell of $AlFeO_3$ used in our simulation contains 8 Fe ions, where the ith Fe ion is connected to the z_i number of the other Fe ions. This gives $J_o = (E_{\rm FM} - E_{\rm AFM})/(\sum_i z_i{}^*8^*|S|^2)$; here, $S = 5/2$ and $E_{\rm FM} - E_{\rm AFM} \approx 1.5$ eV from first-principles calculations. Our estimate of the exchange coupling parameter J_o is ∼6 meV. This value is in good agreement with the one estimated from the two-magnon peak observed in the Raman spectrum here. Denoting $\nabla_{uv}^2 J$ as J_2, the change in phonon frequency Δ of the λth Γ-point phonon mode is given by[20]

$$\Delta_\lambda = \frac{1}{2\mu_\lambda\omega_\lambda}\sum_{\nu}\hat{\vec{u}}_{\nu\Gamma}J_2\hat{\vec{u}}_{\nu\Gamma}. \tag{4}$$

Here, μ_λ and ω_λ are the reduced mass and the frequency of the λth Γ-phonon mode, respectively. Large Δ implies stronger spin coupling.

The calculations are done for both types of disorders: Fe_2 at the Al_2 site (Fe_2-Al_2) and Fe_1 at the Al_2 site (Fe_1-Al_2). For an Fe_2-Al_2–type disorder, Fig. 6(a) and 6(b) shows the changes in Γ-point phonon frequency Δ between FM and AFM states and between NM and AFM states, respectively. The corresponding changes for Fe_1-Al_2 disorder are shown in Fig. 6(c) and 6(d).

To connect our results with our experiment, we listed only those calculated phonon frequencies that are close to the experimentally observed Raman active phonon modes (refer to Table I). We assume the correlation between the experimentally observed modes that exhibit anomalies at the magnetic transition and the calculated spin–phonon coupling

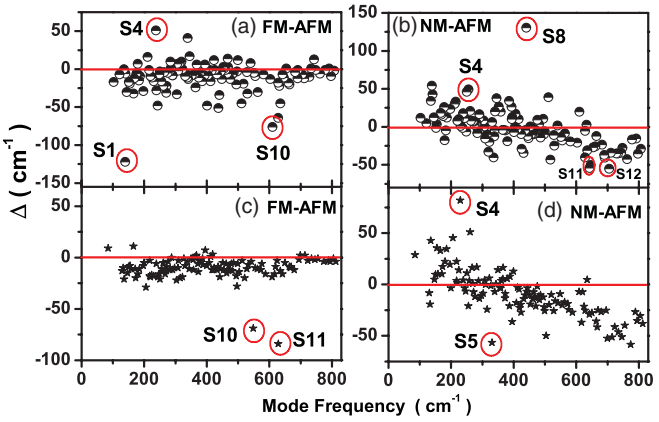

FIG. 6. (Color online) Second-order spin–phonon coupling in different magnetic states. (a) FM-AFM and (b) NM-AFM states with Fe_2-Al_2 antisite disorder. (c) FM-AFM and (d) NM-AFM states with Fe_1-Al_2 antisite disorder.

for modes with frequencies in the vicinity of the observed modes. We then carry out the mode assignment. In the case of Fe_2-Al_2 antisite disorder [Fig. 6(a) and 6(b)], corresponding to correlation between phonons of the FM/NM state with those of the AFM state, Δ and hence J_2 are high for mode frequencies in the neighborhood close to modes S1, S4, and S10 for FM-AFM coupling [Fig. 6(a)] and modes S4, S8, S11, and S12 for NM-AFM coupling [Fig. 6(b)]. For NM-AFM coupling, J_2 is not exactly the spin–phonon coupling parameter as it is in the case of FM-AFM coupling, but here it gives an estimate of the change in phonon frequencies in going from the NM state to AFM ordering. In Fig. 2, modes S4, S7, S8, and S10 show sharp changes in frequency at the transition temperature T_c, suggesting their strong coupling with spin, which is consistent with our first-principles calculations. Another interesting observation from Fig. 6(b) is that the mode with the frequency near S8 shows the largest increase in frequency in going from the AFM to the NM state, which is consistent with our experimental observation of the most significant hardening of mode S8 with an increase in the temperature of the AFM state.

We now discuss the effect of Fe_1-Al_2 antisite disorder that corresponds to changes in frequencies of phonons of the FM [Fig. 6(c)] and NM [Fig. 6(d)] states correlating with those of the AFM state. With the change in magnetic ordering from the FM to the AFM state, modes near S10 and S11 [Fig. 6(c)] exhibit strong second-order coupling with spin. In comparison, modes close to S4 and S5 [Fig. 6(d)] show large second-order coupling for the transition from the NM to the AFM state. Mode S4 was observed in our Raman measurements to exhibit significant hardening across the transition from the AFM to the NM state, consistent with our calculated results.

Our first-principles analysis confirms the existence of strong spin–phonon coupling in $AlFeO_3$ and points out that the anomaly in mode S8 is primarily influenced by Fe_2-Al_2 disorder, while the anomaly in the S4 mode is additionally influenced by Fe_1-Al_2 disorder. Anomalous hardening of the S8 mode is due to strong spin–phonon coupling at the second order (J_2) in $AlFeO_3$.

IV. CONCLUSIONS

We observed strong first-order phonon renormalization below the magnetic transition temperature of $AlFeO_3$ due to strong spin–phonon coupling. In addition, high-frequency Raman bands between 1100 and 1800 cm^{-1} showed pronounced effects of the strong magnetic correlation below T_c. In particular, the intensity of mode S15 becomes zero above the transition temperature T_c; hence, the mode is attributed to two-magnon Raman scattering. The band position gives an estimate of spin exchange constant J_o as $\sim$5.3 meV, in close agreement with the DFT calculations. With first-principles analysis, we explored the effects of magnetic ordering and (Al, Fe) disorder on phonons. Our results suggest a strong interplay between lattice and magnetic degrees of freedom, which are crucial to understanding the underlying physics responsible for the various exotic physical phenomena in these materials. Our Raman data show evidence for a phase transition to a ferroelectric phase below 100 K.

ACKNOWLEDGMENTS

P.K., A.B., and S.N.S. acknowledge the Council of Scientific & Industrial Research, India, for a research fellowship. A.K.S. acknowledges the Department of Science and Technology, India, for financial support. U.V.W. acknowledges the Department of Atomic Energy Outstanding Researcher Fellowship for partial financial support.

*asood@physics.iisc.ernet.in

[1]T. Kimura, T. Goto, H. Shintani, K. Ishizaka, T. Arima, and Y. Tokura, Nature **426**, 55 (2003).
[2]W. Prellier, M. P. Singh, and P. Murugavel, J. Phys.: Condens. Matter **17**, R803 (2005).
[3]S. W. Cheong and M. Mostovoy, Nat. Mater. **6**, 13 (2007).
[4]C. N. R. Rao and C. R. Serrao, J. Mater. Chem. **17**, 4931 (2007).
[5]D. Khomski, Phyics **2**, 20 (2009).
[6]J. H. We, S. J. Kim, and C. S. Kim, IEEE Tran. Mag. **42**, 2876 (1991).
[7]F. Bouree, J. L. Baudour, E. Elbadraoui, J. Musso, C. Laurent, and A. Rousset, Acta. Cryst. B **52**, 217 (1996).
[8]J. Laverdiere, S. Jandl, A. A. Mukhin, V. Y. Ivanov, V. G. Ivanov, and M. N. Iliev, Phys. Rev. B **73**, 214301 (2006).
[9]M. O. Ramirez, A. Kumar, S. A. Denev, Y. H. Chu, J. Seidel, L. Martin, S. Y. Yang, R. C. Rai, X. Xue, J. F. Ihlefeld, N. Podraza, E. Saiz, S. Lee, J. Klug, S. W. Cheong, M. J. Bedzyk, O. Auciello, D. G. Schlom, J. Orenstein, R. Ramesh, J. L. Musfeldt, A. P. Litvinchuk, and V. Gopalan, Appl. Phys. Lett. **94**, 161905 (2009).
[10]P. Kumar, S. Saha, D. V. S. Muthu, J. R. Sahu, A. K. Sood, and C. N. R. Rao, J. Phys.: Condens. Matter **22**, 115403 (2010).

[11]M. Viswanathan, P. S. A. Kumar, V. S. Bhadram, C. Narayana, A. K. Bera, and S. M. Yusuf, J. Phys.: Condens. Matter **22**, 346006 (2010).
[12]K. Sharma, V. R. Reddy, D. Kothari, A. Gupta, A. Banerjee, and V. G. Sathe, J. Phys.: Condens. Matter **22**, 146005 (2010).
[13]S. Mukherjee, R. Gupta, and A. Garg, J. Phys.: Condens. Matter **23**, 445403 (2011).
[14]A. Shireen, R. Saha, S. N. Shirodkar, U. V. Waghmare, A. Sundaresan, and C. N. R. Rao, e-print arXiv:1112.5848v1.
[15]R. Saha, A. Shireen, A. K. Bera, S. N. Shirodkar, Y. Sundarayya, N. Kalarikkal, S. M. Yusuf, U. V. Waghmare, A. Sundaresan, and C. N. R. Rao, J. Solid State Chem. **184**, 494 (2011).
[16]J. P. Perdew, J. A. Chevary, S. H. Vosko, K. A. Jackson, M. R. Pederson, D. J. Singh, and C. Fiolhais, Phys. Rev. B **46**, 6671 (1992).
[17]G. Kresse and J. Hafner, Phys. Rev. B **47**, 558(R) (1993).
[18]G. Kresse and J. Furthmller, Phys. Rev. B **54**, 11169 (1996).
[19]G. Kresse and D. Joubert, Phys. Rev. B **59**, 1758 (1999).
[20]E. Grando, A. García, J. A. Sanjurjo, C. Rettori, I. Torriani, F. Prado, R. D. Sánchez, A. Caneiro, and S. B. Oseroff, Phys. Rev. B **60**, 11879 (1999).
[21]A. P. Litvinchuk, M. N. Iliev, V. N. Popov, and M. M. Gospodinov, J. Phys.: Condens. Matter **16**, 809 (2004).
[22]H. Fukumara, N. Hasuike, H. Harima, K. Kisoda, K. Fukae, T. Yoshimura, and N. Fujimura, J. Phys.: Condens. Matter **21**, 064218 (2009).
[23]P. Kumar, S. Saha, C. R. Serrao, A. K. Sood, and C. N. R. Rao, Pramana J. Phys. **74**, 281 (2010).
[24]M. J. Massey, U. Baier, R. Merlin, and W. H. Weber, Phys. Rev. B **41**, 7822 (1990).
[25]S. J. Allen and H. J. Guggenheim, Phys. Rev. Lett. **21**, 1807 (1968).
[26]I. W. Shepherd, Phys. Rev. B **5**, 4524 (1972).
[27]M. O. Ramirez, M. Krishnamurthi, S. Denev, A. Kumar, S. Y. Yang, Y. H. Chu, E. Saiz, J. Seidel, A. P. Pyatakov, A. Bush, D. Viehland, J. Orenstein, R. Ramesh, and V. Gopalan, Appl. Phys. Lett. **92**, 022511 (2008).
[28]P. A. Fleury, J. M. Worlock, and H. J. Guggenheim, Phys. Rev. **185**, 738 (1969).
[29]C. H. Perry, E. Anastassakis, and J. Sokoloff, Indian J. Pure Appl. Phys. **9**, 930 (1971).
[30]M. N. Iliev, A. P. Litvinchuk, M. V. Abrashev, V. N. Popove, J. Cmaidalka, B. Lorenz, and R. L. Meng, Phys. Rev. B **69**, 172301 (2004).